

Lateral heterogeneity effects on Rayleigh wave dispersion: Investigation on numerically simulated MASW frameworks

S. BIGNARDI¹, N. Abu Zeid¹, G. Santarato¹

¹Department of Earth Sciences, University of Ferrara, Ferrara (Italy)

Introduction

Seismic surface wave methods gained popularity during the last decade to retrieve the shallow subsurface shear wave velocity (V_s) from the analysis of the recorded wave field.

Besides early approaches, such as the Spectral Analysis of Surface Waves (Nazarian and Stokoe, 1984; Stokoe et al., 1994), based on a two-receiver setup and the passive methods (Louie, 2001; Rix et al., 2002; Park et al., 2005), based on noise recordings which are not investigated here, the “Multi-channel Analysis of Surface Waves” method known as MASW, which exploits an array of receivers (see for e.g. Gabriels, 1987; Tokimatsu, 1995; Tselentis and Delis, 1998; Park et al., 1999) is up to date one of the most widely adopted non-invasive active-source approaches in the professional world for the evaluation of the stiffness properties of the ground for geotechnical engineering purposes and represent the starting point for many research fields. The method utilizes the dispersive nature of either Rayleigh and Love waves excited by an active source and recorded by a sensors array along a profile on the ground surface. Surface waves propagation allows for the construction of the dispersion curve which is then inverted to obtain the shear wave velocity profile (Park et al., 1999; Socco and Strobbia, 2004). Dispersion curves generation requires the transformation of the recorded datasets i.e. the seismograms, from the time-space domain into a more suitable domain for the analysis, typically the frequency-wave number ($f-k$) or the frequency-velocity ($f-V$) domain where experimental dispersion curves of the propagating modes are extracted by locating the local maxima during the so-called picking operation. Finally, the misfit between theoretical and experimental dispersion curves is minimized during the inversion procedure. Available inversion algorithms assume the subsurface model as a stack of homogeneous parallel layers, so that they can only capture the vertical distribution of elastic properties of the subsurface model i.e. they are 1-D. (see, e. g. Aki, 2002; Kausel and Roessel, 1981); however this is only a convenient approximation of the actual subsurface conditions for most sites and it may yield misleading results if the actual soil profile is far from the assumed geometry.

Up to date there is a growing trend toward applications of MASW for spatially 2-D imaging and many attempts are being done to mitigate the 1-D limitation, especially focusing on the inversion procedure. Among these approach, the so called “pseudo-2D inversion” (e.g. Luo et al., 2008; Boiero and Socco, 2010), where successive 1-D inversions are combined along the length of the survey profile via interpolation or other type of smoothing kernel and the Multi-offset Phase Analysis (MOPA) (Strobbia and Foti, 2006; Vignoli et al., 2011), where lateral discontinuities can be recognized and portions of the model, considered parallel layered, are inverted separately. Even successful, these strategies still remain based on a 1-D forward model, which is inherently limited. On the other hand, little work has been done on the forward model side. To overcome the limitations of the 1-D forward model involves necessarily the use of more general modeling techniques (Virieux et al., 2011) capable of taking into account the lateral heterogeneities. These modeling approaches however are more effective when coupled to Full Waveform Inversion (FWI)

which represent an alternative approach to surface waves interpretation which allow for the direct inversion of either time or frequency domain datasets avoiding the picking procedure which is prone to errors due to human interpretation of the transformed domain. FWI gained popularity for reservoir investigation (Virieux and Operto, 2009) and application to the geotechnical scale still is a young field of research (Bignardi, 2011; Bignardi et al. 2012; Tran and Hiltunen, 2012). Despite its limitations, classic MASW approach still remain of value when the subsoil can be considered subhorizontal.

In this paper we investigate the effects of lateral heterogeneities such as variations of layers thickness on the f-V transform to assess the limitations and judge the reliability of traditional surface waves interpretation. To do so, we investigate the vertical component of accelerations computed by our newly developed three-dimensional (3-D) elastodynamic solver based on the Spectral Element Method (Komatitsch, 1998; Komatitsch, 1999; Meza-Fajardo, 2008), for a 48 channels array with 1 meter channel spacing, 30 meters offset and generated by a point source located at the surface of a two layer model with the following properties: $\rho_1 = 1000 \text{ kg/m}^3$, $Vs_1 = 100 \text{ m/s}$, $Vp_1 = 500 \text{ m/s}$ over an half space ($\rho_2 = 1500 \text{ Kg/m}^3$, $Vs_2 = 750 \text{ m/s}$, $Vp_2 = 160 \text{ m/s}$), where ρ is the material density, Vs is the shear wave velocity and Vp is the compression wave velocity. Source time variation is given by a 18 Hz central frequency Ricker wavelet. The forward modeling was carried out considering both a ramp model with different slopes (β) of the interface and a ramp model with a strong discontinuity. The obtained seismograms were transformed into the f-V domain where the influence of different interface slopes β is investigated and compared to the Hermann's theoretical modes for the neighboring left (L-condition) and right (R-condition) flat layered conditions. Finally, different locations of a strong lateral variation are compared.

Data Processing

By following the classic MASW approach, we consider the seismograms as representing a dataset in the time-space domain which have to be transformed into a more suitable domain. Prior of any elaboration however, each time-series is windowed with an Hanning window in order both to decrease the influence of body waves on the dispersion curve and to clean the seismograms where they are expected to be flat from any numerical noise and any backscattered residual not adsorbed by the Stacey's adsorbing boundary condition (Komatitsch and Tromp, 1999) and by the Anisotropic Perfectly Matched Layer (Zheng and Huang, 2002). To obtain the f-V transform we followed Lin (2007) and applied a discrete time Fourier transform (DTFT, see equation 1), followed by the discrete space Fourier transform DSFT in equation 2 . The DTFT

$$A(f_j, x_n) = \frac{1}{M} \sum_{m=0}^{M-1} a(t_m, x_n) \exp(-2i\pi f_j t_m) , \quad (1)$$

where $a(t, x)$ is the acceleration, m n and j are integer indexes that identify the time sample of the digitalized acceleration, the receiver position and a particular frequency respectively; i is the imaginary unit and each time-series is assumed M samples long and collected at the sampling frequency $F_s = 1/\Delta t = 1000 \text{ s}^{-1}$. Equation 1 is exploited to translate each seismogram in the frequency-offset domain (SFT), where each dataset can be viewed as a collection of harmonic functions of space. This domain is particularly suitable to display the effects due to the presence of

a lateral heterogeneity. The frequency-velocity transform (FVT) is finally retrieved performing a Discrete Space Fourier Transform on (1),

$$Y(f_j, V) = \sum_{n=0}^{N-1} A(f_j, x_n) \exp\left(-2i\pi \frac{f_j}{V} x_n\right) , \quad (2)$$

where N is the number of receivers along the array and $x_n = n \Delta x$ with $\Delta x = 1 \text{ m}$. With the representation (1, 2) it is possible to produce high quality dispersion curves; furthermore, it can be demonstrated that f-V, f-k or the p-τ transformed domains are completely equivalent (Lin and Lin, 2007).

Discussion

Concerning the MASW method, it is well known that the array length L is usually chosen based on a compromise between depth of investigation and resolution of the final dispersion curve. Indeed, for the presented Vs profile model a good trade-off is represented by an array of geophones at 1 meter of distance between each other. Furthermore, in order to allow for a good separation of the modes (Socco and Strobbia, 2004) and still to investigate arrays exploited in the professional world we chose to investigate a 48 channels array. The case of vertical interface between two quarter-spaces or the step transition were already investigated in 2-D approximation (Lin and Lin, 2007) exploiting the finite differences method, so we limit to simulations of the interface slope to a maximum of 45 degrees.

The flat layered model we investigated is depicted on top of the first column of Fig. 1, and models corresponding to the presence of the slope follow in the same column. Wave propagation is simulated with the source located 30 m to the left of the array. First and last receivers are indicated with the ∇ symbol to allow for comparison between the horizontal extent of the slope to the array length L. Columns 2 and 3, in Fig. 1, show the frequency-velocity transform calculated as a function of the increasing slope by applying equations 1 and 2 to the seismograms. For sake of comparison theoretical dispersion curves, calculated by using Herrmann's software are, superposed to the simulated transforms for both the flat models corresponding to the left and right part of the subsurface in column 2 and 3 respectively. Indeed, for the Ricker source we adopted a meaningful frequency band, i.e. the frequency band in which elastic energy is not negligible between 0 and 50 Hz and in this range the FVT represents the dynamic information of the propagation. The intensity in the FVT at a certain location (f, V) corresponds to the amplitude of the harmonic plane wave $A(f, V) \exp(ik_x x - i\omega t)$ and so it is also an indication of the energy carried by that wave. Indeed, for a flat model (first row of Fig. 1) the FVT transform of the 48 channels array matches the theoretical dispersion curves pretty well. When the slope is weak ($\beta \leq 10^\circ$), the lateral heterogeneity could be considered as a perturbation to the flat model so that changes in the frequency-velocity domain undergo weak changes. Percent differences in wave amplitudes between the FVT corresponding to the flat left model and sloping models are shown in Fig. 2 according to

$$\Delta Y(\beta) = (Y_{flat} - Y_\beta) / \max(Y_{flat}) .$$

Red colour corresponds to a loss in amplitude, while blue colour corresponds to an increase, so that it is apparent how the energy leaks toward a perturbed version of the propagating modes. When

slope is stronger, see the third row of Fig. 1 ($\beta = 15^\circ$), the subsurface geometry corresponds to a sloping model followed by a portion corresponding to the right flat condition. In this situation the energy distribution corresponds to a combination of modes perturbation and to a jump of elastic energy toward modes pertaining to the right flat condition. Inspecting Fig. 2 however, we can see that part of the energy jumps towards the first left higher mode. Finally, when slopes are stronger ($\beta \geq 30^\circ$), the portion of “right flat model” beneath the array is comparable to the array extent and so the elastic energy mainly propagates accordingly to the theoretical modes calculated for the right flat model. Fig. 2 shows that the transition is sharp.

As a final observation, in all the examples presented in Figs. 1 and 2 the slope started in correspondence to the first receiver; as a result the subsurface model beneath the array corresponds to a sloping portion and a portion that corresponds to R-condition. As previously stated, the most the slope angle β increases the most the subsurface beneath the array is similar to the R-condition. On the other hand we pointed out that in case of ($\beta \geq 30^\circ$) the transition is sharp, so it is worthy to investigate the influence of different sharp transition locations.

Fig. 3 depicts the FVT and SFT for a strong lateral heterogeneity scenario ($\beta = 45^\circ$) as a function of the slope location. It can be noted that the portion of energy that jumps from the L-condition modes to the R-condition modes greatly depends on the portion of R-condition flat model under the array and that the pattern in FVT resemble some weighted combination of the theoretical modes expected at the left and Right of the transition. Indeed, this was observed also in Vignoli et al. (2011) for arrays of hundreds of receivers. Further, the SFT reveals a non stationary property in the space domain and oscillated interference features can be observed on the left of slope even when a small portion of the L-condition model is present. Indeed, such interference patterns were previously observed by Lin and Lin (2007) for the vertical transition: in our simulation they are still present when the interface is $\beta \geq 15^\circ$ even if the maximum amplitude of reflected waves we observed was in the worst of cases a few percent of the incident wave amplitude.

Conclusions

In this paper we discussed effects of subsurface lateral variation on the frequency-velocity transform on a classical MASW setup. In order to allow for a good separation of the modes and still to investigate arrays exploited in the professional world we chosen to investigate a 48 channels array. Acceleration at the receivers placed on the surface of a three-dimensional two layers (layer + half-space) simplified model were computed for different slopes of the interface between the top layer and the half space. The vertical component of the accelerograms were Hanning windowed and then transformed using the discrete-time and discrete-space Fourier transform to retrieve the simulated frequency-velocity transforms as a function of the slope β . The obtained FVT were then compared to the multi-modal Rayleigh wave dispersion curve obtained by using Herrmann’s software. Discrete time Fourier transform allows for the identification of lateral heterogeneity by inspecting the frequency-offset domain where interference phenomena and changes in the wave amplitude patterns arise even for slopes $\beta < 30^\circ$. These interferences however were not associated to strong back-reflections and in the worst of cases back-reflected wave amplitudes accounted for a few percent of the incident wave amplitude. As such, in case of sloping interface and up to $\beta < 45^\circ$ back reflection does not seems to significantly affect the FVT plot.

Furthermore, when considering different interface slopes, FVT is weakly affected when the slope can be considered a perturbation with respect to the flat model and this translates into a weak fixed frequency perturbation of the modes.

At moderate slopes ($15^\circ < \beta < 30^\circ$) the subsurface consists of a sloping part and a R-condition flat part. The FVT shows a perturbation of the modes and a jump of the energy to locations of the FVT corresponding to the first L-condition higher mode and to the R-condition mode fundamental.

Finally when a strong transition is investigated as a function of the location of the sloping part, the energy seems to distribute on a pattern that is to some extent a weighted combination of the flat models beneath the array. This is in agreement with what previously stated by Vignoli et al. (2011) for long arrays except that here a sloped interface was introduced. Presence of the slope however only seems to account for a perturbation of the energy pattern. It is worth noting that this aspect supports for the use of local approximation such as the coupling mode method or the MOPA for the use of the pseudo 2-D interpretation.

Finally, for the case of Fig. 3 (first row), where the top layer suddenly thickens just before the first receivers, energy distributes on the theoretical modes of the R-condition flat model: this leads us to the conclusion that data collected by the array are weakly sensitive to heterogeneities that are not directly beneath the receivers.

Figures

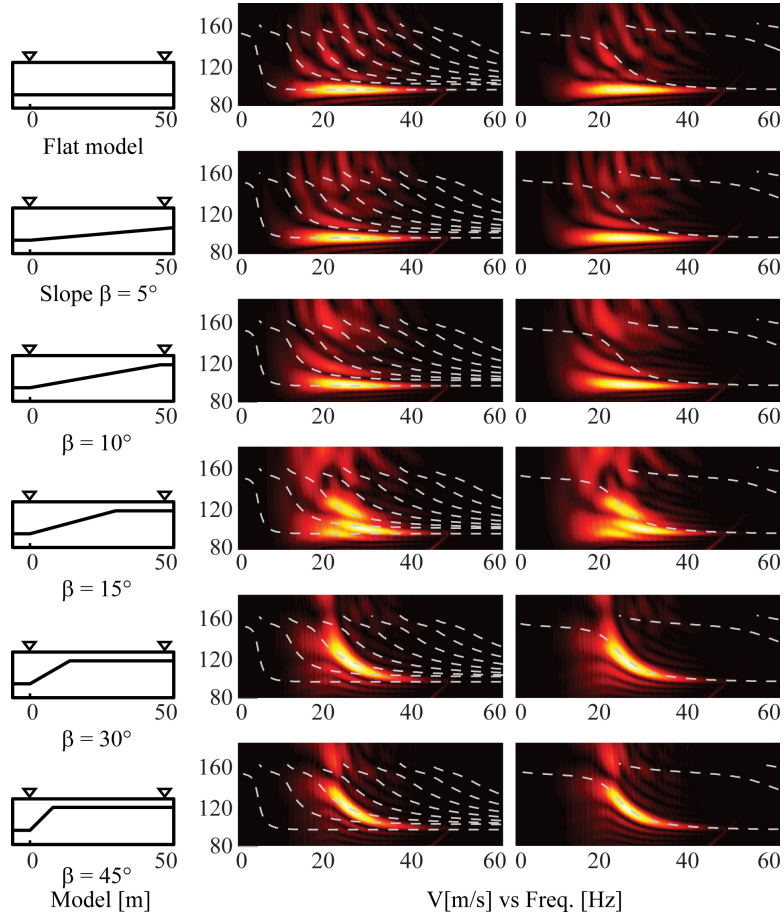


Fig. 1: Col. 1: Subsurface models with transition from left (L) to right (R) parallel layer condition. Col. 2-3: f-V transform as a function of slope compared to Herrmann's modes for L-R condition respectively.

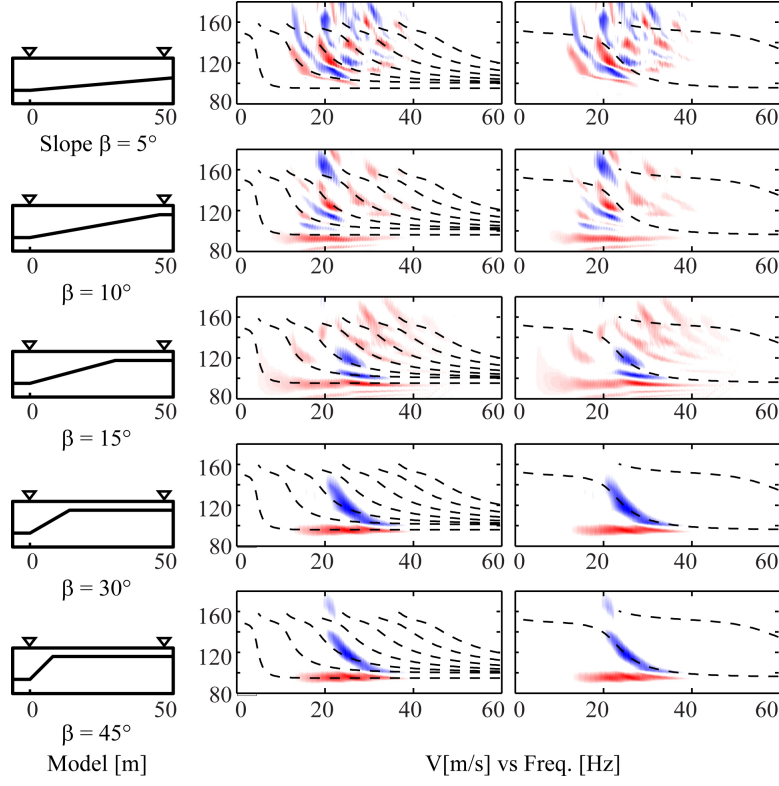


Fig. 2: Col. 1: Subsurface models with transition from left (L) to right (R) parallel layer condition. Col. 2-3: normalized difference of f-V transform between sloped and flat model as a function of slope compared to Herrmann's modes for L-R condition respectively.

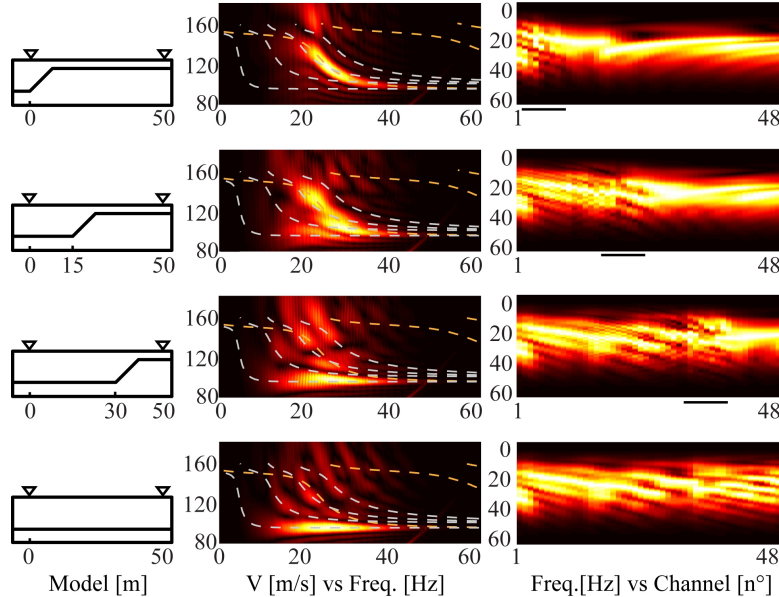


Fig. 3: Col. 1: Subsurface models with transition from left (L) to right (R) parallel layer condition and different positions of a 45° transition. Col. 2: f-V transform as function of slope compared to

Herrmann's modes for L (grey), and R (orange) conditions; Col 3. Frequency-offset transforms; the black line below each image indicates position and horizontal extent of the transition.

References

- Aki K. and Richards P. G.; 2002: *Quantitative seismology, Theory and methods* (second edition), University Sciences Books, Sausalito, California, pp. 700.
- Bignardi S., Fedele, F., Yezzi, A. J., Rix, G. J. and Santarato G.; 2012: *Geometric seismic wave inversion by the boundary element method.*, Bull. Seismol. Soc. Am. **102**, 802-811.
- Bignardi S.; 2011: *Complete waveform inversion approach to seismic surface waves and adjoint active surfaces*, PH. D. Thesis in Earth Sciences, University of Ferrara, Ferrara, Italy.
- Boiero D. and Socco L. V.; 2010: *Retrieving lateral variations from surface waves dispersion curves*. Geophysical Prospecting, **58**, pp. 977-996.
- Gabriels P., Snieder R. and Nolet G.; 1987: *In situ measurements of shear-wave velocity in sediments with higher-mode Rayleigh waves*. Geophysical Prospecting, **35**, pp.187-196.
- Herrmann R. B.; Computer Programs in Seismology. Saint Louis University, Version 3.30.
- Kausel E. and Roessel J. M.; 1981: *Stiffness matrices for layered soils*. Bull. Seism. Soc. Am. **71**, pp. 1743-1761.
- Komatitsch D. and Tromp J.; 1999: *Introduction to the spectral element method for three-dimensional seismic wave propagation*. Geophys. J. Int., **139**, pp. 806-822.
- Komatitsch D. and Villotte J. P.; 1998: *The spectral element method: An efficient tool to simulate the seismic response of 2d and 3d geological structures*. Bull. Seis. Soc. Am., **88** (2), pp. 368-392.
- Lin C. P. and Lin C. H.; 2007: *Effect of lateral heterogeneity on surface wave testing: Numerical simulations and a countermeasure*. Soil Dyn. Earthq. Eng., **27**, pp. 541-552.
- Louie J. N.; 2001: *Faster, better: shear-wave velocity to 100 meters depth from refraction microtremor arrays*. Bull. Seism. Soc. Am. **91** (2) pp. 347-364.
- Luo Y. H., Xia J. H., Liu J. P., Xu Y. X. and Liu Q. S.; 2008: *Generation of a pseudo-2d shear-wave velocity section by inversion of a series of 1D dispersion curves*. J. Appl. Geophysics, **64**, pp. 115-124.
- Meza-Fajardo K. C. and Papageorgiou A. S.; 2008: *The spectral element method (SEM): formulation and implementation of the method for engineering seismology problems*. The XIV World Conference on Earthquake Engineering, Beijing, China.
- Nazarian S. and Stokoe K. H.; 1984: *In situ shear wave velocity from spectral analysis of surface wave.*, Proceedings of the 8th Conference on Earthquake engineering, St. Francisco, Prentice Hall, **3** pp. 31-38.
- Park C. B., Miller R. D., Ryden N., Xia J. and Ivanov J.; 2005: *Combined use of active and passive surface waves*. J. Env. Eng. Geophys. **10**, pp. 323-334.

- Park C. B., Miller R. D. and Xia J.; 1999: *Multichannel analysis of surface waves*: Geophysics, **64** (3), pp. 800-808.
- Rix G. J., Hebeler G. L. and Orozco M. C.; 2002: *Near-surface Vs profiling in the New Madrid seismic zone using surface wave methods*. Seismol. Res. Lett. **73** (3) pp. 380-392.
- Socco L. V. and Strobbia C.; 2004: *Surface-wave method for near-surface characterization: a tutorial*. Near Surface Geophysics, 2, pp. 165-185.
- Stokoe K. H., Wright S. G., Bay J. A. and Roesset J. M.; 1994: *Characterization of geotechnical sites by SASW method*. Proceedings of the XIII International Conference on Soil Mechanics and Foundation Engineering, Oxford & IBH Publishing, New Delhi, pp. 15-25.
- Strobbia C. and Foti S.; 2006: *Multi-offset phase analysis of surface wave data (MOPA)*. J. Appl. Geophys., **59**, pp .300-313.
- Tokimatsu K.; 1995: *Geotechnical site characterization using surface waves*. Proceedings of the 1st International Conference on Earthquake Geotechnical Engineering (IS-Tokyo '95), Balkema, Rotterdam, The Netherlands, pp. 1333-1368.
- Tran K. T. and Hiltunen D. R.; 2012: *Shear Wave Velocity via Inversion of Full Waveforms*. Proceedings of Geocongress 2012, Oakland (CA), ASCE Geotechnical Special Publication, **225**, pp. 2766-2775.
- Tselentis G. A. and Delis G.; 1998: *Rapid assessment of S-wave profiles from the inversion of multichannel surface wave dispersion data*. Annali di Geofisica **41**, pp. 1-15.
- Vignoli G., Strobbia C., Cassiani G. and Vermeer P.; 2011: *Statistical multioffset phase analysis for surface-wave processing in lateral varying media*. Geophysics, **76** (2), pp. U1--U11.
- Virieux J., Calandra H. and Plessix R. E.; 2011: *A review of the spectral, pseudo-spectral, finite-difference and finite-element modeling techniques for geophysical imaging*. Geophysical Prospecting, **59**, pp. 794-813.
- Virieux J. and Operto S.; 2009: *An overview of full-waveform inversion in exploration geophysics*. Geophysics, **74** (6) pp. 127-152.
- Zheng Y. and Huang X.; 2002: *Anisotropic Perfectly Matched Layers for Elastic Waves in Cartesian and Curvilinear Coordinates*. Report at Massachusetts Institute of Technology.